Journal of Computational and Applied Mathematics 235 (2010) 491–506

Contents lists available at ScienceDirect

Journal of Computational and Applied Mathematics

journal homepage: www.elsevier.com/locate/cam

Roe solver with entropy corrector for uncertain hyperbolic systems☆

J. Tryoen [a,b,1], O. Le Maître [b], M. Ndjinga [c], A. Ern [a,*]

[a] Université Paris Est, CERMICS, Ecole des Ponts, 77455 Marne la Vallée cedex 2, France

[b] LIMSI-CNRS, 91403 Orsay cedex, France

[c] CEA-Saclay, DEN, DM2S, SFME, F-91191 Gif-sur-Yvette, France

ARTICLE INFO

Article history:
Received 30 October 2009
Received in revised form 26 March 2010

Keywords:
Uncertainty quantification
Hyperbolic systems
Conservation laws
Stochastic spectral methods
Galerkin projection
Roe solver
Entropy correction

ABSTRACT

This paper deals with intrusive Galerkin projection methods with a Roe-type solver for treating uncertain hyperbolic systems using a finite volume discretization in physical space and a piecewise continuous representation at the stochastic level. The aim of this paper is to design a cost-effective adaptation of the deterministic Dubois and Mehlman corrector to avoid entropy-violating shocks in the presence of sonic points. The adaptation relies on an estimate of the eigenvalues and eigenvectors of the Galerkin Jacobian matrix of the deterministic system of the stochastic modes of the solution and on a correspondence between these approximate eigenvalues and eigenvectors for the intermediate states considered at the interface. We derive some indicators that can be used to decide where a correction is needed, thereby reducing the computational costs considerably. The effectiveness of the proposed corrector is assessed on the Burgers and Euler equations including sonic points.

1. Introduction

To date, most computer simulations have been based on deterministic mathematical models, where all input data are assumed to be perfectly known. In fact, this is seldom the case. A great challenge in recent years has been to provide effective tools for uncertainty quantification and propagation, that is, to quantify the resulting uncertainty in the numerical solution due to the uncertainty in input data (such as model parameters, initial and boundary conditions, and geometry). Stochastic spectral methods and so-called chaos expansions originally introduced in [1] provide such tools by parametrizing the uncertain input data by means of random variables with known distribution functions and expanding the stochastic solution in a basis of (orthogonal) polynomials associated with the chosen random variables. The determination of the stochastic modes of the solution can then be achieved by non-intrusive methods based on the use of the numerical code solving the deterministic model for a sampling of the random variable or by a stochastic Galerkin projection of the model equation yielding a reformulated deterministic problem for the stochastic modes of the solution. Such methods have been successfully applied to a large variety of engineering problems governed by elliptic, parabolic or ordinary differential equations. Two specific difficulties for the application of such methods to uncertain hyperbolic systems are the development of discontinuities in the solution in both physical and stochastic spaces and the nonlinearities in the flux functions. Different approaches have been proposed relying on multi-element probabilistic collocation methods [2], ENO-like reconstructions [3], pseudo-intrusive methods where the stochastic modes of the flux are computed by quadrature

☆ This work was partially supported by GNR MoMaS (ANDRA, BRGM, CEA, EdF, IRSN, PACEN-CNRS). O.P. Le Maître is partially supported by the French National Research Agency (Grant ANR-08-JCJC-0022).

* Corresponding author at: Université Paris Est, CERMICS, Ecole des Ponts, 77455 Marne la Vallée cedex 2, France.
E-mail addresses: tryoenj@cermics.enpc.fr (J. Tryoen), olm@limsi.fr (O. Le Maître), michael.ndjinga@cea.fr (M. Ndjinga), ern@cermics.enpc.fr (A. Ern).
1 Tel.: +33 1 64 15 36 65.

0377-0427/$ – see front matter © 2010 Elsevier B.V. All rights reserved.
doi:10.1016/j.cam.2010.05.043

methods [4,5], and fully intrusive methods using generalized Polynomial Chaos (gPC) methods in the case of the scalar linear wave equation [6] and Multi-Element-gPC (ME-gPC) methods in the case of nonlinear hyperbolic problems with relatively small fluctuations of the random quantities [7].

We proposed in [8] a fully intrusive method for treating nonlinear hyperbolic systems using a Finite Volume (FV) discretization in physical space and a piecewise continuous representation [9–11] at the stochastic level. To this end the stochastic space is discretized using tensor-product stochastic elements supporting local polynomial bases, and a stochastic Galerkin projection is applied to the original stochastic hyperbolic problem to derive the Galerkin system, that is, the set of deterministic equations coupling the stochastic modes of the solution. The nonlinear fluxes in the Galerkin system are computed in a pseudo-spectral way with the tools described in [12]. Furthermore, a cost-effective Roe-type solver for the Galerkin system has been designed in [8] using an upwinding determined from an approximate spectrum of the Galerkin Jacobian matrix evaluated at a suitable Roe state. This matrix is referred to as the Roe Galerkin Jacobian matrix. Numerical tests on the stochastic Burgers and Euler equations (without sonic points) in one spatial dimension and, respectively, in two and one stochastic dimensions (number of stochastic variables) indicated that the method is accurate and robust while maintaining moderate computational costs.

Nevertheless, while effectively stabilizing the numerical method, the Roe scheme is known in the deterministic case to yield unphysical (entropy-violating) solutions in the presence of sonic points. In such a situation, a corrector is needed to construct numerical fluxes consistent with the physics. As in the deterministic case, non-physical expansion shocks occur in the stochastic case in the vicinity of sonic points; this is illustrated in the numerical experiments presented below. In the literature, different entropy correctors have been proposed for the Roe scheme. The most used are those due to Harten [13] and Roe [14] and consist in adding a linear diffusive term in situations where the linearized Roe flux leads to an entropy-violating solution. In fact, these corrections appear more as "spreading devices" which act upon the approximate solution rather than a remedy for the fact that the approximate flux is linear in situations where a nonlinear description is crucial. The Dubois and Mehlman (DM) corrector is more general because it consists in a nonlinear modification of the flux in the vicinity of sonic points. Moreover, this corrector is non-parametric.

The aim of the present paper is to propose a cost-effective adaptation of the deterministic DM corrector to the Roe-type solver outlined above. Direct application of the DM corrector to the Roe solver for the Galerkin system is not straightforward. First, the DM corrector needs the reconstruction of the intermediate states corresponding to each couple of left and right states at each interface cell in the physical domain and therefore the knowledge of the eigenvectors of the Roe Galerkin Jacobian matrix. The dimension of the Galerkin system can be quite large and we want to avoid the actual spectral decomposition of the Galerkin Jacobian matrix. Moreover, the DM corrector assumes a strictly hyperbolic system, while this is generally not the case for the Galerkin system, where eigenvalues with multiplicity larger than 1 are common, leading to difficulties in defining the intermediate states. To overcome these issues, we can use Theorem 3 in [8] to obtain an inexpensive estimate of the eigenvectors of the Roe Galerkin Jacobian matrix and an explicit correspondence between the approximate spectrum and the approximate eigenvectors of the Roe Galerkin Jacobian matrix for the various intermediate states. These facts play a central role herein in adapting the DM corrector to the present setting. A further important ingredient is that the Galerkin Jacobian matrix is block diagonal owing to the choice of piecewise continuous representation in the stochastic space. As a result, we can apply the DM corrector independently in each stochastic element. Finally, we study different indicators that can be used to decide where the correction is actually needed, thereby achieving a substantial reduction of computational costs.

The paper is organized as follows. In Section 2, we briefly recall the Galerkin projection of stochastic hyperbolic systems and the Roe-type solver introduced in [8]. The adaptation of the DM entropy corrector to the Galerkin system is described in Section 3. Simulations results are presented in Section 4. We adopt the following notation: lower case symbols represent deterministic quantities, whereas upper case symbols represent stochastic quantities.

2. Galerkin projection of stochastic hyperbolic systems and the Roe-type solver

2.1. Stochastic hyperbolic systems

We are interested in stochastic nonlinear hyperbolic systems with uncertain input quantities that can be parametrized for simplicity with N independent identically distributed random variables $\xi := \{\xi_1, \ldots, \xi_N\}$ uniformly distributed in $\Xi := [0,1]^N$. Let us denote as $p_\xi = 1$ the density function of ξ and let $L^2(\Xi, p_\xi)$ be the space of second-order random variables defined on the probability space $\mathcal{P}_\xi := (\Xi, \mathcal{B}_\Xi, p_\xi)$, where $\mathcal{B}_\Xi$ is the Borel set of Ξ. The expectation operator in $\mathcal{P}_\xi$ is denoted for any random variable $H(\xi)$ defined on $\mathcal{P}_\xi$ by $\langle H \rangle := \int_\Xi H(y) p_\xi(y) dy$. Let $(x, t, \xi) \in \Omega \times [0, T] \times \Xi$, where Ω is the physical domain and T the simulation time. We seek $U(x, t, \xi) \in \mathcal{A}_U \otimes L^2(\Xi, p_\xi)$, solving almost surely the following conservative system:

$$\begin{cases} \dfrac{\partial}{\partial t} U(x,t,\xi) + \dfrac{\partial}{\partial x} F(U(x,t,\xi);\xi) = 0, \\ U(x, t=0, \xi) = U^0(x,\xi), \end{cases} \tag{1}$$

where $\mathcal{A}_U \subset \mathbb{R}^m, m \geq 1$ is the set of admissible values for the solutions of the deterministic version of (1), and $F(U;\xi) \in \mathbb{R}^m \otimes L^2(\Xi, p_\xi)$ is the stochastic flux vector. For instance, for the one-dimensional Euler system, $m = 3$, the components of U are the density, the impulse, and the total energy, and $\mathcal{A}_U$ corresponds to the states for which the density and pressure are positive. The stochastic system (1) is assumed to be hyperbolic in the sense that the stochastic Jacobian matrix $\nabla_U F \in \mathbb{R}^{m,m} \otimes L^2(\Xi, p_\xi)$ is $\mathbb{R}$-diagonalizable almost surely.

2.2. Stochastic discretization

We discretize the stochastic space Ξ using tensor-product stochastic elements, resulting from successive dyadic partitions of Ξ, and supporting local polynomial bases; we approximate the solution in the stochastic space of fully tensorized piecewise polynomial functions $\mathcal{S}^{\mathrm{No,Nr}}$, where $\mathrm{Nr} \geq 0$ denotes the resolution level (controlling the size $2^{-\mathrm{Nr}}$ of the stochastic elements) and $\mathrm{No} \geq 0$ denotes the expansion order (controlling the degree of the piecewise polynomial approximation in each variable ξ_i); see the details in [10]. Therefore, the space $\mathcal{S}^{\mathrm{No,Nr}}$ has dimension

$$\dim \mathcal{S}^{\mathrm{No,Nr}} = \mathrm{P}_\pi \mathrm{P}_\sigma =: \mathrm{P}, \tag{2}$$

where $\mathrm{P}_\pi := (\mathrm{No}+1)^{\mathrm{N}}$ is the dimension of the local polynomial basis on each stochastic element, and $\mathrm{P}_\sigma := 2^{\mathrm{NNr}}$ is the number of stochastic elements.

We use throughout this paper the so-called Stochastic Element (SE) basis to span $\mathcal{S}^{\mathrm{No,Nr}}$, which corresponds to local fully tensorized (rescaled) Legendre polynomial bases such that the approximate solution in $\mathcal{S}^{\mathrm{P}} := \mathcal{S}^{\mathrm{No,Nr}}$ is expanded as a series in the form

$$U(x,t,\xi) \approx U^{\mathrm{P}}(x,t,\xi) = \sum_{\alpha=1}^{\mathrm{P}} u_\alpha(x,t)\Psi_\alpha(\xi), \tag{3}$$

where the deterministic $\mathbb{R}^m$-valued fields $u_\alpha(x,t)$ are called the stochastic modes of the solution (in $\mathcal{S}^{\mathrm{P}}$) and $\{\Psi_\alpha\}_{\alpha=1,\dots,\mathrm{P}}$ denotes the SE basis. In practice, α represents a double index $(\alpha_\sigma, \alpha_\pi)$, where α_σ refers to the stochastic element and α_π to the polynomial function in the stochastic element.

2.3. The Galerkin system

Projecting (1) on the SE basis, we obtain the Galerkin system which couples all the stochastic modes in the form

$$\begin{cases} \dfrac{\partial}{\partial t}u(x,t) + \dfrac{\partial}{\partial x}f(u(x,t)) = 0, \\ u(x,t=0) = u^0(x), \end{cases} \tag{4}$$

where $u(x,t) = (u_1(x,t),\dots,u_{\mathrm{P}}(x,t))^T \in \mathbb{R}^{m\mathrm{P}}$, and $f(u(x,t)) = (f_1(u),\dots,f_{\mathrm{P}}(u))^T \in \mathbb{R}^{m\mathrm{P}}$ are respectively the vector of the stochastic modes and the Galerkin flux vector with

$$f_\alpha(u) \equiv \left\langle \Psi_\alpha F\left(U^{\mathrm{P}};\cdot\right)\right\rangle, \quad \alpha = 1,\dots,\mathrm{P}, \quad \text{and} \quad U^{\mathrm{P}} = \sum_{\beta=1}^{\mathrm{P}} u_\beta \Psi_\beta(\xi). \tag{5}$$

Moreover, $u^0 = \left(\left\langle \Psi_\alpha U^0\right\rangle\right)_{\alpha=1,\dots,\mathrm{P}}$. The component vector u must belong to the admissible set $\mathcal{A}_u \subset \mathbb{R}^{m\mathrm{P}}$ such that $u \in \mathcal{A}_u \Leftrightarrow U^{\mathrm{P}}(\xi) = \sum_{\alpha=1}^{\mathrm{P}} u_\alpha \Psi_\alpha(\xi) \in \mathcal{A}_U \otimes L^2(\Xi, p_\xi)$. The Galerkin Jacobian matrix of order $m\mathrm{P}$ defined as

$$(\nabla_u f(u))_{\alpha,\beta=1,\dots,\mathrm{P}} = \left\langle \nabla_U F(U^{\mathrm{P}};\cdot)\Psi_\alpha\Psi_\beta\right\rangle_{\alpha,\beta=1,\dots,\mathrm{P}} \tag{6}$$

has a diagonal block structure owing to the decoupling of the problem over different stochastic elements. In particular, for a given stochastic element α_σ, $1 \leq \alpha_\sigma \leq \mathrm{P}_\sigma$, the corresponding diagonal block of size $\mathrm{P}_\pi \times \mathrm{P}_\pi$ is denoted by $[\nabla_u f]^{\alpha_\sigma}$. In the sequel, all the developments are performed on each stochastic element independently. We consider the approximate Galerkin Jacobian matrix $\overline{\nabla_u f}$ which is also block-diagonal and such that for each stochastic element α_σ, $1 \leq \alpha_\sigma \leq \mathrm{P}_\sigma$, the coefficients of the corresponding block $\left[\overline{\nabla_u f}\right]^{\alpha_\sigma}$ are obtained by approaching the coefficients of $[\nabla_u f]^{\alpha_\sigma}$ by a Gauss quadrature in the form

$$\left(\left[\overline{\nabla_u f}(u)\right]^{\alpha_\sigma}\right)_{\alpha_\pi,\beta_\pi=1,\dots,\mathrm{P}_\pi} = \left(\sum_{\gamma=1}^{\mathrm{P}_\pi} \varpi_\gamma \nabla_U F(U^{\mathrm{P}}(\xi_\gamma);\xi_\gamma)\Psi_{\alpha_\sigma,\alpha_\pi}(\xi_\gamma)\Psi_{\alpha_\sigma,\beta_\pi}(\xi_\gamma)\right)_{\alpha_\pi,\beta_\pi=1,\dots,\mathrm{P}_\pi}, \tag{7}$$

where $\{\xi_\gamma\}_{\gamma=1,\dots,\mathrm{P}_\pi}$ is the set of the Gauss points of the stochastic element α_σ, with associated weights $\{\varpi_\gamma\}_{\gamma=1,\dots,\mathrm{P}_\pi}$. To simplify the notation, we drop the superscript α_σ. An important result is that the matrix $\overline{\nabla_u f}$ is $\mathbb{R}$-diagonalizable with

eigenvalues and right and left eigenvectors given by

$$\begin{cases} \lambda'_{k\eta} = \Lambda^k(\xi_\eta), & \forall k = 1,\dots,m,\ \eta = 1,\dots,\mathrm{P}_\pi, \\ \left(r'_{k\eta}\right)_{\beta=1,\dots,\mathrm{P}_\pi} = \left(\varpi_\eta R^k(\xi_\eta)\Psi_\beta(\xi_\eta)\right)_{\beta=1,\dots,\mathrm{P}_\pi}, & \forall k = 1,\dots,m,\ \eta = 1,\dots,\mathrm{P}_\pi, \\ \left(l'_{k\eta}\right)_{\beta=1,\dots,\mathrm{P}_\pi} = \left(\varpi_\eta L^k(\xi_\eta)\Psi_\beta(\xi_\eta)\right)_{\beta=1,\dots,\mathrm{P}_\pi}, & \forall k = 1,\dots,m,\ \eta = 1,\dots,\mathrm{P}_\pi, \end{cases} \tag{8}$$

where $\{\Lambda(\xi)\}_{k=1,\dots,m}$, $\{R^k(\xi)\}_{k=1,\dots,m}$ and $\{L^k(\xi)\}_{k=1,\dots,m}$ are respectively the eigenvalues and right and left eigenvectors of $\nabla_U F(U^{\mathrm{P}}(\xi);\xi)$. This fact is proven in [8]; for completeness, we outline the proof in Appendix A. The $\mathbb{R}$-diagonalization of the matrix $\overline{\nabla_u f}$ has important consequences. First, using as in [8] the spectrum of $\overline{\nabla_u f}$ to approximate the spectrum of $\nabla_u f$ allows us to compute efficiently upwind matrices for Roe-type solvers; this procedure is briefly outlined in Section 2.4. Moreover, using the eigenvectors of $\overline{\nabla_u f}$ to approximate the eigenvectors of $\nabla_u f$ allows us to extend the DM entropy corrector to the present setting; this extension is described in Section 3.

To shorten the notation, it is convenient to use a single index for the eigenvalues and eigenvectors in the form $\{\lambda'_\gamma\}_{\gamma=1,\dots,m\mathrm{P}_\pi}$, $\{r'_\gamma\}_{\gamma=1,\dots,m\mathrm{P}_\pi}$, and $\{l'_\gamma\}_{\gamma=1,\dots,m\mathrm{P}_\pi}$. The prime indicates that these quantities approximate their counterpart associated with $\overline{\nabla_u f}$.

2.4. A Roe-type solver without entropy correction

The Galerkin system (4) is discretized in physical space and time using a FV method in the form

$$u_i^{n+1} = u_i^n - \frac{\Delta t^n}{\Delta x}\left(\varphi(u_i^n, u_{i+1}^n) - \varphi(u_{i-1}^n, u_i^n)\right), \tag{9}$$

where u_i^n is an approximation to the cell average in physical space of the solution u in the cell of center $i\Delta x$ with width Δx at the discrete time t^n and $\varphi(\cdot,\cdot)$ is the Galerkin numerical flux.

The method presented in [8] is based on a Roe-type solver without entropy correction. As in the deterministic context, it can be viewed as an approximate Riemann solver where the Galerkin flux $f(u)$ is replaced at each interface LR separating left and right states (u_L, u_R) by the linear approximation

$$f^{\mathrm{Roe}}(u_L, u_R, u) = f(u_L) + a(u_L, u_R)\cdot(u - u_L), \tag{10}$$

where $a(u_L, u_R)$ is a Roe linearized approximation of the Galerkin Jacobian matrix. To define $a(u_L, u_R)$, we assume that the original stochastic problem (1) possesses a Roe state $U_{LR}^{\mathrm{Roe}}(\xi)$ on each interface LR separating left and right stochastic states $(U_L(\xi), U_R(\xi))$ such that $\nabla_U F(U_{LR}^{\mathrm{Roe}}(\xi))$ is a Roe linearized matrix for the stochastic problem. Then, the matrix

$$a(u_L, u_R) := a_{LR}^{\mathrm{Roe}} := \left\langle \nabla_U F(U_{LR}^{\mathrm{Roe}};\cdot)\Psi_\alpha\Psi_\beta\right\rangle_{\alpha,\beta=1,\dots,\mathrm{P}} \tag{11}$$

is a Roe linearized matrix for the Galerkin problem [8] under the assumption that this matrix is $\mathbb{R}$-diagonalizable. The Galerkin numerical flux is chosen in the form

$$\varphi(u_L, u_R) \equiv \varphi^{\mathrm{Roe}}(u_L, u_R) = \frac{f(u_L) + f(u_R)}{2} - |a_{LR}^{\mathrm{Roe}}|\frac{u_R - u_L}{2}. \tag{12}$$

Furthermore, so as to avoid the expensive spectral decomposition of the Roe Galerkin Jacobian matrix a_{LR}^{Roe} needed to compute its absolute value, we proposed in [8] approximating $|a_{LR}^{\mathrm{Roe}}|$ by a polynomial transformation $q_{d,\{\lambda'\}}$ applied to a_{LR}^{Roe}. This polynomial transformation is conveniently determined independently in each stochastic element α_σ, $1 \le \alpha_\sigma \le \mathrm{P}_\sigma$, using the approximate spectrum $\{\lambda'_\gamma\}_{\gamma=1,\dots,m\mathrm{P}_\pi}$ of $\left[a_{LR}^{\mathrm{Roe}}\right]^{\alpha_\sigma}$ and minimizing the least-squares error $\sum_{\gamma=1}^{m\mathrm{P}_\pi}\left(|\lambda'_\gamma| - q_{d,\{\lambda'\}}(\lambda'_\gamma)\right)^2$. Finally, the time step Δt^n is computed using a CFL-type condition in the form

$$\frac{\Delta t^n}{\Delta x} = \frac{\mathrm{CFL}}{\max\limits_{LR\in\mathcal{L},\gamma=1,\dots,m\mathrm{P}_\pi}|\lambda'_\gamma(u_{LR}^{\mathrm{Roe}})|}, \tag{13}$$

where $\mathcal{L}$ denotes the set of interfaces LR and CFL denotes a user-dependent parameter ≤ 1. When working with more than one stochastic element, (13) yields a local time step $\Delta t_{\alpha_\sigma}^n$, $1 \le \alpha_\sigma \le \mathrm{P}_\sigma$, for each stochastic element, and the global time step is selected as $\Delta t^n = \min_{1\le\alpha_\sigma\le\mathrm{P}_\sigma}\Delta t_{\alpha_\sigma}^n$.

The above methodology has been extensively tested and analyzed in [8] on the stochastic Burgers and Euler equations without sonic points. It can be expected that an entropy corrector is needed as in the deterministic case to prevent entropy-violating shocks across sonic points. Test cases will effectively illustrate this point in Section 4.

3. DM-type entropy correction

In this section, we propose an entropy correction for the above Roe-type solver based on an adaptation to the present context of the non-parametrized entropy corrector proposed in [15].

3.1. General principles of the DM corrector

The methodology of Dubois and Mehlman holds for general deterministic hyperbolic systems. It consists in adding a correction to the numerical Roe flux to avoid entropy-violating shocks, the correction relying on a nonlinear modification of the numerical flux in the vicinity of sonic points. The detection and treatment of such shocks involve three steps. First, the eigenvalues corresponding to the Roe state at each physical interface separating left and right states are put in increasing order, and the corresponding eigenvectors of the Roe Galerkin Jacobian matrix are ordered accordingly. Secondly, the components of the difference between the left and right states in the eigenvector basis are determined, and suitable intermediate states are computed. Finally, a sonic expansion wave is detected between the $(i-1)$-th and i-th intermediate states if the i-th eigenvalue corresponding to the $(i-1)$-th intermediate state is negative whereas the i-th eigenvalue corresponding to the i-th intermediate state is positive. In this case, a nonlinear modification of the Roe numerical flux φ^{Roe} is added. An important aspect of the DM corrector is a correspondence between the sets of eigenvalues for all the intermediate states. This is reflected by the fact that the DM corrector has been applied to strictly hyperbolic deterministic systems where the Jacobian matrix $\nabla_u f$ has real distinct eigenvalues and a complete set of linearly independent eigenvectors. Moreover, the left and right states at each interface are assumed to be sufficiently close (see [15, Theorem 6.1]) so that the correspondence between the eigenvalues can be achieved through a common reference state.

We present now the direct application of the DM corrector to the numerical scheme of Section 2.4. At each interface LR of the physical space with left and right states u_L and u_R respectively, we assume for the time being that the Roe Galerkin Jacobian matrix $\left[a_{LR}^{\mathrm{Roe}}\right]^{\alpha_\sigma}$ associated with the stochastic element α_σ, $1 \le \alpha_\sigma \le \mathrm{P}_\sigma$, is $\mathbb{R}$-diagonalizable with distinct eigenvalues. Then, we can write $\left[a_{LR}^{\mathrm{Roe}}\right]^{\alpha_\sigma} = \sum_{\gamma=1}^{m\mathrm{P}_\pi} \lambda_\gamma(u_{LR}^{\mathrm{Roe}}) l_\gamma(u_{LR}^{\mathrm{Roe}}) \otimes r_\gamma(u_{LR}^{\mathrm{Roe}})$ with eigenvalues $(\lambda_\gamma)_{\gamma=1,\dots,m\mathrm{P}_\pi}$, left eigenvectors $(l_\gamma)_{\gamma=1,\dots,m\mathrm{P}_\pi}$, and right eigenvectors $(r_\gamma)_{\gamma=1,\dots,m\mathrm{P}_\pi}$. The detection of the sonic points needs to build the $(m\mathrm{P}_\pi+1)$ intermediate states $(u_\gamma)_{\gamma=0,\dots,m\mathrm{P}_\pi}$ such that

$$
\begin{aligned}
&u_0 = u_L\\
&u_\gamma = u_{\gamma-1} + \beta_\gamma r_\gamma(u_{LR}^{\mathrm{Roe}}) \quad \gamma = 1,\dots,m\mathrm{P}_\pi\\
&u_R = u_{m\mathrm{P}_\pi}
\end{aligned}
$$

where $(\beta_\gamma)_{\gamma=1,\dots,m\mathrm{P}_\pi}$ are the components of the vector $u_R - u_L$ in the basis of right eigenvectors,

$$
u_R - u_L = \sum_{\gamma=1}^{m\mathrm{P}_\pi} \beta_\gamma r_\gamma(u_{LR}^{\mathrm{Roe}}). \tag{14}
$$

Then, the set of sonic indices is $S := \{\gamma, \lambda_\gamma(u_{\gamma-1}) < 0 < \lambda_\gamma(u_\gamma)\}$ and an interface is said to be sonic if S is non-empty. We modify $f^{\mathrm{Roe}}(u_L, u_R, u)$ only at sonic interfaces. To this end, we introduce the following modified flux function parametrized by u_L and u_R:

$$
f^{\mathrm{DM}}(u_L, u_R, u) = f(u_L) + \sum_{\gamma=1}^{m\mathrm{P}_\pi} g_\gamma(w_\gamma(u)) r_\gamma(u_{LR}^{\mathrm{Roe}}), \tag{15}
$$

where $(w_\gamma(u))_{\gamma=1,\dots,m\mathrm{P}_\pi}$ are the characteristic variables defined by

$$
u - u_L = \sum_{\gamma=1}^{m\mathrm{P}_\pi} w_\gamma(u) r_\gamma(u_{LR}^{\mathrm{Roe}}).
$$

The functions $(g_\gamma)_{\gamma=1,\dots,m\mathrm{P}_\pi}$ are parametrized by the intermediate states $(u_\gamma)_{\gamma=1,\dots,m\mathrm{P}_\pi}$ and are defined according to

$$
\begin{aligned}
&\text{if } \gamma \notin S,\ \forall w, \quad g_\gamma(w) = \lambda_\gamma(u_{LR}^{\mathrm{Roe}}) w,\\
&\text{if } \gamma \in S, \quad g_\gamma(w) = \begin{cases} p_\gamma(w) & \forall w \in (0, \beta_\gamma),\\ \lambda_\gamma(u_{LR}^{\mathrm{Roe}}) w & \forall w \notin (0, \beta_\gamma), \end{cases}
\end{aligned}
$$

where p_γ is the unique Hermite polynomial of degree 3 defined by the conditions

$$
p_\gamma(0) = 0, \qquad p_\gamma(\beta_\gamma) = \lambda_\gamma(u_{LR}^{\mathrm{Roe}})\beta_\gamma, \qquad p'_\gamma(0) = \lambda_\gamma(u_{\gamma-1}), \qquad p'_\gamma(\beta_\gamma) = \lambda_\gamma(u_\gamma).
$$

Elementary algebra shows that $p_\gamma(w) = aw^3 + bw^2 + cw$ with

$$
a = \frac{\lambda_\gamma(u_\gamma) + \lambda_\gamma(u_{\gamma-1}) - 2\lambda_\gamma(u_{LR}^{\mathrm{Roe}})}{\beta_\gamma^2}, \qquad b = \frac{3\lambda_\gamma(u_{LR}^{\mathrm{Roe}}) - 2\lambda_\gamma(u_{\gamma-1}) - \lambda_\gamma(u_\gamma)}{\beta_\gamma}, \qquad c = \lambda_\gamma(u_{\gamma-1}).
$$

Away from sonic points, the modified flux f^{DM} coincides with the linearized Roe flux f^{Roe}. Finally, the modified Galerkin numerical flux $\varphi^{\mathrm{DM}}(u_L, u_R)$ has the expression

$$
\varphi^{\mathrm{DM}}(u_L, u_R) = \varphi^{\mathrm{Roe}}(u_L, u_R) + \sum_{\gamma\in S} \max\left\{ \frac{g_\gamma(w_\gamma^\star)}{\beta_\gamma}, \frac{g_\gamma(w_\gamma^\star)}{\beta_\gamma} - \lambda_\gamma(u_{LR}^{\mathrm{Roe}}) \right\} \beta_\gamma r^\gamma(u_{LR}^{\mathrm{Roe}}), \tag{16}
$$

where

$$w_\gamma^\star = \frac{-\lambda_\gamma(u_{\gamma-1})\beta_\gamma}{3\lambda_\gamma(u_{LR}^{\mathrm{Roe}}) - 2\lambda_\gamma(u_{\gamma-1}) - \lambda_\gamma(u_\gamma) + \sqrt{(3\lambda_\gamma(u_{LR}^{\mathrm{Roe}}) - \lambda_\gamma(u_\gamma) - \lambda_\gamma(u_{\gamma-1}))^2 - \lambda_\gamma(u_{\gamma-1})\lambda_\gamma(u_\gamma)}}$$

is the value for which g_γ reaches its unique extremum in $(0, \alpha_\gamma)$.

3.2. Adaptation to the Galerkin system

An important point is that the Galerkin system is generally not strictly hyperbolic, i.e., some eigenvalues are multiple. Moreover, for practical reasons, we want to avoid the need for the actual spectral decomposition of the diagonal blocks of the Galerkin Jacobian matrix since the size of these blocks is still quite large. To this end, we consider for left and right states (u_L, u_R) and the associated Roe Galerkin Jacobian matrix $\left[a_{LR}^{\mathrm{Roe}}\right]^{\alpha\sigma}$, the approximate eigenvalues $\{\lambda'_\gamma\}_{\gamma=1,\dots,m\mathrm{P}_\pi}$ and the corresponding approximate eigenvectors $\{r'_\gamma\}_{\gamma=1,\dots,m\mathrm{P}_\pi}$ defined by (8). We build the $(m\mathrm{P}_\pi + 1)$ approximate intermediate states $(u'_\gamma)_{\gamma=0,\dots,m\mathrm{P}_\pi}$ such that

$$\begin{aligned} u'_0 &= u_L \\ u'_\gamma &= u'_{\gamma-1} + \beta'_\gamma r'_\gamma(u_{LR}^{\mathrm{Roe}}) \quad \gamma = 1, \dots, m\mathrm{P}_\pi \\ u_R &= u'_{m\mathrm{P}_\pi} \end{aligned}$$

where $(\beta'_\gamma)_{\gamma=1,\dots,m\mathrm{P}_\pi}$ are the components of the vector $u_R - u_L$ on the basis of approximate eigenvectors $(r'_\gamma(u_{LR}^{\mathrm{Roe}}))_{\gamma=1,\dots,m\mathrm{P}_\pi}$. A key ingredient is that the numbering of the approximate eigenvalues and eigenvectors in the Roe approximate state via the Gauss points enables us to construct the correspondence between the eigenvalues of the various intermediate states, and consequently to determine the set of the sonic indices $S = \{\gamma, \lambda'_\gamma(u'_{\gamma-1}) < 0 < \lambda'_\gamma(u'_\gamma)\}$ in a coherent way. We can then modify the Roe numerical flux $\varphi^{\mathrm{Roe}}(u_L, u_R)$ defined by (12) as described above.

4. Results

4.1. Test case 1: the Burgers equation

The purpose of this test case is to assess the method on the stochastic scalar conservation law of Burgers in the case where a sonic point is present almost surely. We compare the numerical solution with the exact solution and study the spatial convergence of the method. A comparison with a Monte Carlo method is also presented.

4.1.1. Problem definition

We consider the Burgers equation

$$\frac{\partial U}{\partial t} + \frac{\partial F(U)}{\partial x} = 0, \quad F(U) = \frac{U^2}{2}, \tag{17}$$

with stochastic initial condition $U^0(x, \xi)$ defined using two uncertain states, the first one almost surely negative and the second one almost surely positive. We take for $x \in [0, 1]$,

$$U^0(x, \xi) = \begin{cases} U^-(\xi_1) & x < 1/2, \\ U^+(\xi_2) & x \geq 1/2, \end{cases} \tag{18}$$

with

$$\begin{aligned} U^-(\xi_1) &= -1 + 0.05(2\xi_1 - 1), \qquad \xi_1 \sim \mathcal{U}[0, 1] \to U^- \sim \mathcal{U}[-1.05, -0.95], \\ U^+(\xi_2) &= 1 + 0.1(2\xi_2 - 1), \qquad \xi_2 \sim \mathcal{U}[0, 1] \to U^+ \sim \mathcal{U}[0.9, 1.1]. \end{aligned} \tag{19}$$

Therefore, the problem has two stochastic dimensions ($\mathrm{N} = 2$). The initial condition is illustrated in Fig. 1. The stochastic Burgers equation is time-integrated using the methodology described above. Unless specified, $\mathrm{Nc} = 250$ cells are used for space discretization with a CFL constant set to 0.95 in (13), and the stochastic parameters are $\mathrm{No} = 3$ for the expansion order and $\mathrm{Nr} = 3$ for the resolution level so that the dimension of the stochastic approximation space is $\dim \mathcal{S}^{\mathrm{No,Nr}} = (\mathrm{No} + 1)^{\mathrm{N}} 2^{\mathrm{NNr}} = 1024$. Since $m = 1$ here, the Galerkin system is of size 1024. The computation of the nonlinear flux $F(U)$ relies on spectral methods as detailed in [8].

For the random initial conditions specified by (19) and setting $t_s := \frac{x-1/2}{t}$, the (exact) stochastic entropy solution of the Burgers equation consists in an expansion wave whose expression can be easily derived for $t > 0$ and $\xi = (\xi_1, \xi_2) \in [0, 1]^2$:

$$U^{ex}(x, t, (\xi_1, \xi_2)) = \begin{cases} U^-(\xi_1) & t_s \leq U^-(\xi_1), \\ t_s & U^-(\xi_1) < t_s < U^+(\xi_2), \\ U^+(\xi_2) & t_s \geq U^+(\xi_2). \end{cases} \tag{20}$$

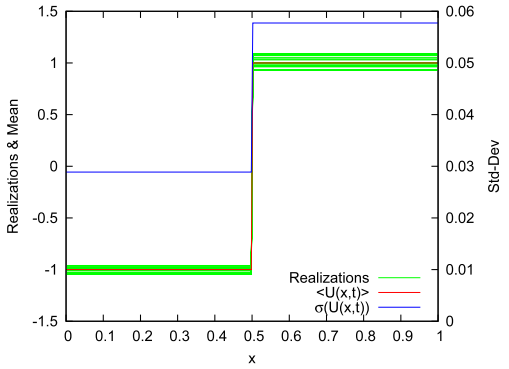

Fig. 1. Random initial condition for test case 1: a sample set of 20 random realizations, the mean, and the standard deviation. The scale on the right is for the standard deviation.

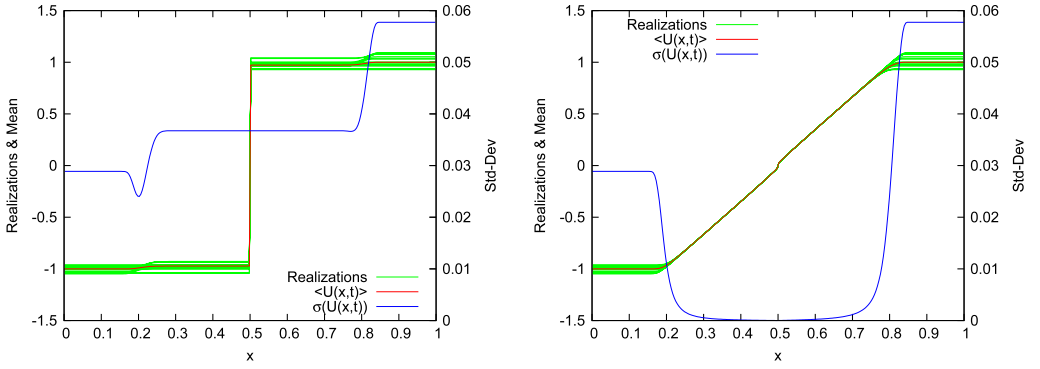

Fig. 2. Stochastic solution of the Burgers equation at $t = 0.3$ obtained without (left) and with (right) the entropy corrector. The solution mean and standard deviation are plotted as a function of x, together with a reconstruction of 20 randomly generated realizations of the solution. The scale on the right is for the standard deviation.

An important remark is that the solution is independent of the uncertainty for (x, t) such that

$$\sup_{\xi_1 \in [0,1]} U^-(\xi_1) < t_s < \inf_{\xi_2 \in [0,1]} U^+(\xi_2), \tag{21}$$

so the standard deviation vanishes for $x \in I(t)$ with $I(t) := [-0.95t + 0.5, 0.9t + 0.5]$. Moreover, it is readily verified that the mean and standard deviation of the exact solution are both piecewise affine functions in physical space at all times.

4.1.2. Numerical results

We compare in Fig. 2 the stochastic solution at $t = 0.3$ obtained without the entropy corrector (left) and with the corrector proposed above (right). The solution expectation and standard deviation, together with a random sample set of realizations, are plotted. The realizations are reconstructed from the stochastic expansions of the solutions using a unique set of randomly generated realizations of $\xi \in [0, 1]^2$. As in the deterministic case, we observe in the left panel of Fig. 2 that the Roe-type solver without entropy corrector does not capture the entropy solution of the problem. In fact, it captures an entropy-violating shock together with small perturbations due to the fact that the right and left initial states are almost surely non-symmetric. With the additional entropy correction proposed above, the entropy solution is well-captured, as shown in the right panel of Fig. 2. Moreover, we have verified that the sonic points of the Galerkin system are, as in the deterministic case, detected only for the interface located at $x = 0.5$. In fact, the uncertainty is not very important for this test case, so all the sonic waves have the same physical location almost surely for the times that we consider. In addition, the set of sonic indices in a stochastic element corresponding to $x = 0.5$ turns out to have cardinality $(\mathrm{No} + 1)^2$, meaning that all the eigenvalues of the Galerkin Jacobian matrix change their sign at the interface and consequently all the components of the Galerkin numerical flux need to be supplemented with an entropy correction.

In Fig. 3, the two first moments of the computed solution are compared with the two first moments of the exact solution for two different choices of the parameter CFL. It is seen that the means of the computed and exact solutions are in agreement in the two cases, although, as in the deterministic case, a slight jump remains at $x = 0.5$ for the computed mean. The standard deviation is correctly captured by our method: it is almost zero on an interval included in $I(t = 0.3) = [0.215, 0.77]$ (where the exact standard deviation is zero). However, significant errors remain in the vicinity of $x = 0.2$ and $x = 0.8$ especially for the case $\mathrm{CFL} = 0.7$ since the Roe-type scheme causes a spreading of the numerical solution in physical space. This issue can be partly handled by increasing the CFL constant, as reflected in the right panel of Fig. 3.

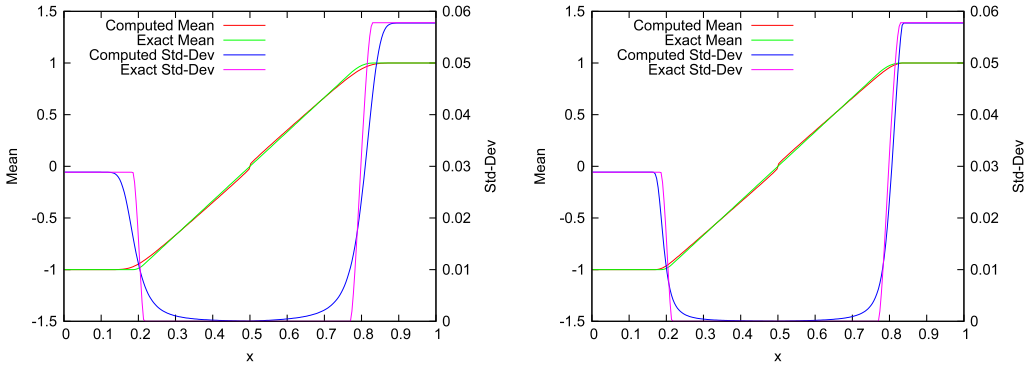

Fig. 3. Stochastic Burgers equation: comparison of the mean and standard deviation of the numerical solution at $t = 0.3$ with the corresponding mean and standard deviation of the exact solution for CFL $= 0.7$ (left) and CFL $= 0.99$ (right).

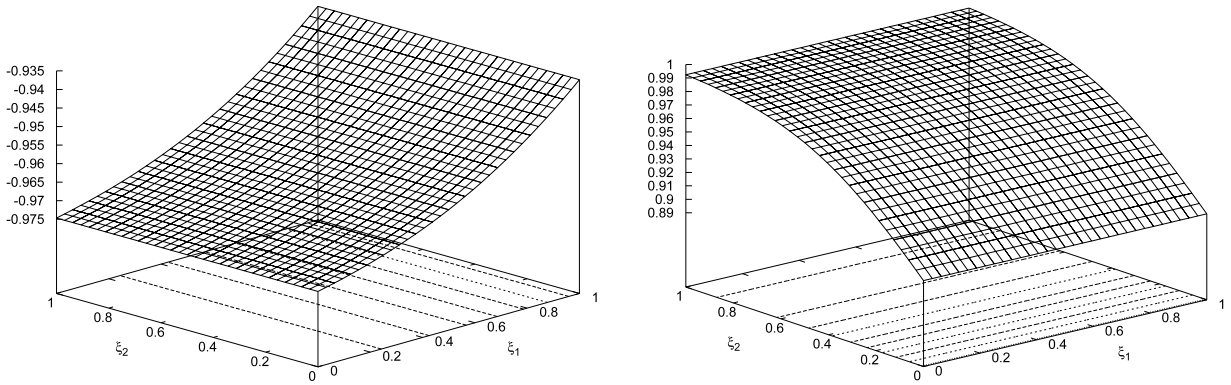

Fig. 4. Stochastic solution of the Burgers equation as a function of (ξ_1, ξ_2) at $t = 0.3$ and $x = 0.2$ (left) or $x = 0.8$ (right).

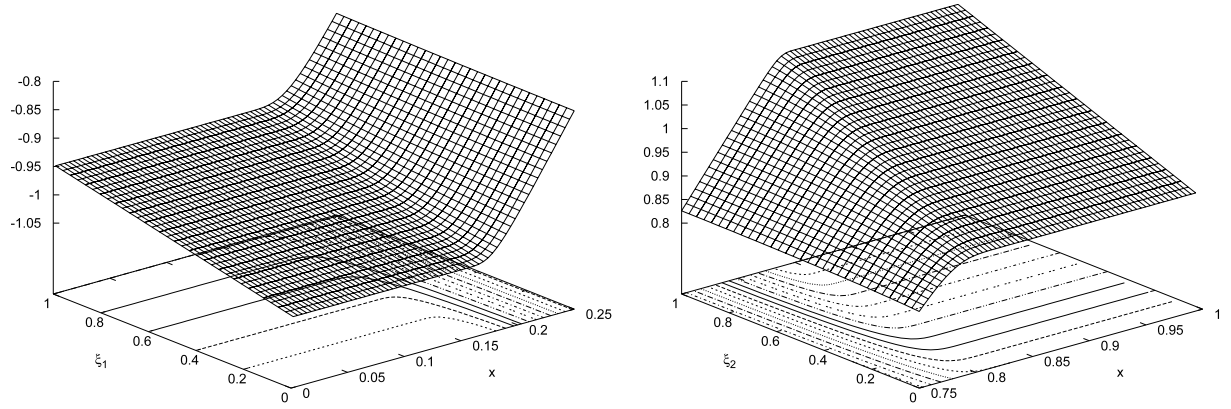

Fig. 5. Stochastic solution of the Burgers equation at $t = 0.3$ as a function of (x, ξ_1) for $0 \le x \le 0.25$ (left) and (x, ξ_2) for $0.75 \le x \le 1$ (right).

A further interesting observation is that the numerical solution depends almost surely only on ξ_1 for $x < 0.5$ and only on ξ_2 for $x > 0.5$, as does the exact solution. This is shown in Fig. 4 where the stochastic solution $U(x, t, \xi)$ is plotted as a function of $\xi = (\xi_1, \xi_2)$ for $x = 0.2$ (left) and $x = 0.8$ (right). In Fig. 5, we represent the stochastic solution at $t = 0.3$ as a function of (x, ξ_1) for $0 \le x \le 0.25$ (left) and as a function of (x, ξ_2) for $0.75 \le x \le 1$ (right). This figure confirms the validity of the stochastic expansion since the stochastic solution is smooth as expected. In addition, it corroborates the use of a polynomial degree No > 1 to correctly represent the nonlinearity of the solution with respect to the stochastic variable.

The jump which remains in the vicinity of the sonic point at $x = 0.5$ is expected as in the deterministic case, because the numerical solver is first order. Since the standard deviation of the solution is almost surely zero at the center of the domain, the jump coincides with the value obtained in the deterministic case almost surely. The jump can consequently be represented in the left panel of Fig. 6 as a function of the spatial step by taking the difference between the values of the

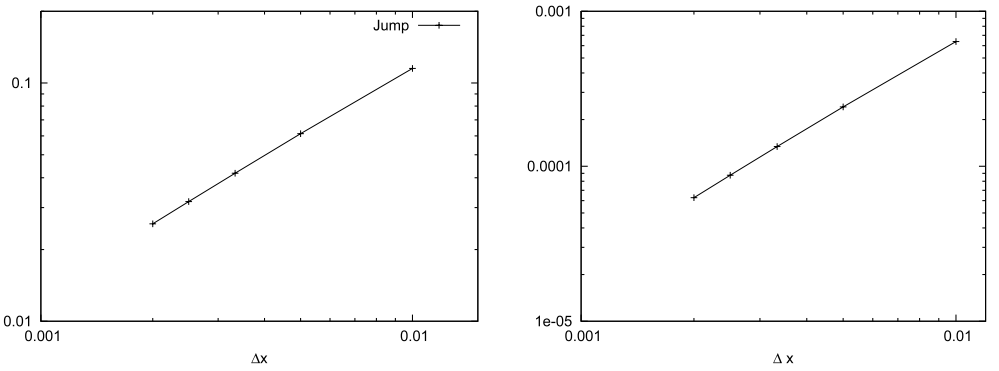

Fig. 6. Left: value of the jump of the numerical solution as a function of the spatial step Δx. Right: stochastic error ϵ^2_{ex} as a function of the spatial step Δx. Computations at $t = 0.3$.

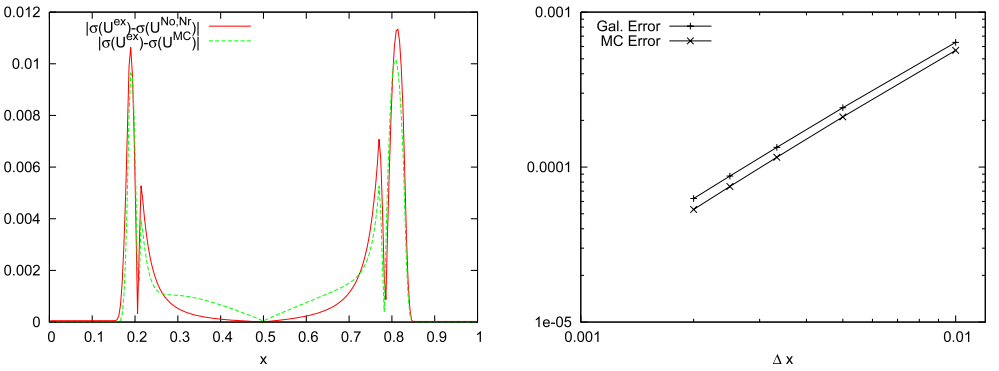

Fig. 7. Left: difference between the standard deviation of the exact solution and the Galerkin solution compared with the difference between the standard deviation of the exact solution and the MC solution. Right: stochastic errors ϵ^2_{ex} and $\epsilon^2_{ex,\mathrm{MC}}$ as a function of the spatial step Δx for the Galerkin solution and the MC solution. The presented results correspond to $t = 0.3$.

mean of the computed solution on the right cell and on the left cell of the interface located at $x = 0.5$. It decreases linearly with the spatial step; this is the same behavior as in the deterministic case.

To further analyze the spatial convergence of the method, we consider the error measure

$$\epsilon^2_{ex}(t) \equiv \frac{1}{M}\sum_{i=1}^{M}\sum_{j=1}^{\mathrm{Nc}} \Delta x \left(U_j^{\mathrm{No,Nr}}(t,\xi^{(i)}) - U^{ex}(x_j,t,\xi^{(i)})\right)^2, \tag{22}$$

where, for each element $\xi^{(i)}$ in a sample set, $U_j^{\mathrm{No,Nr}}(t,\xi^{(i)})$ and $U^{ex}(x_j,t,\xi^{(i)})$ are respectively evaluated from the computed solution at the cell j in physical space and from the exact solution of the corresponding deterministic problem at the center of the cell j in physical space. We use a sample set of size $M = 100\,000$ uniformly drawn from Ξ. The right panel of Fig. 6 reports the error ϵ^2_{ex} at time $t = 0.3$ as a function of the spatial step. We observe a linear decay rate of the error because the spatial error largely dominates in this test case where the solution is smooth in both physical and stochastic spaces.

4.1.3. Comparison of the Galerkin method with a Monte Carlo method

We finally compare the Galerkin solution with a Monte Carlo (MC) solution obtained from the resolution of 100 000 deterministic problems, each of these problems corresponding to a realization of ξ in a sample set. The two methodologies yield different results, as shown in Fig. 7. In the left panel, the absolute value of the difference between the standard deviation of the exact solution and that of the Galerkin solution is compared with the absolute value of the difference between the standard deviation of the exact solution and that of the MC solution. We notice that the Galerkin method yields better results than the MC method in the vicinity of the sonic point at $x = 0.5$. Indeed, the standard deviation does not vanish for the MC method because the latter considers a time step Δt specific to each realization of ξ, thereby creating a variability of the jump at $x = 0.5$. The Galerkin method considers the same time step Δt for all the stochastic elements (see the discussion after (13)), and therefore overcomes these difficulties by introducing some numerical diffusion. However, this diffusion creates numerical errors in the vicinity of $x = 0.2$ and $x = 0.8$ which are more important than for the MC method. As a further

comparison, we consider the MC error measure

$$\epsilon^2_{ex,\mathrm{MC}}(t) \equiv \frac{1}{M}\sum_{i=1}^{M}\sum_{j=1}^{\mathrm{Nc}} \Delta x \left(U_j^{\mathrm{MC}}(t,\xi^{(i)}) - U^{ex}(x_j,t,\xi^{(i)})\right)^2, \tag{23}$$

where, for each element $\xi^{(i)}$ in a sample set, $U_j^{\mathrm{MC}}(t,\xi^{(i)})$ and $U^{ex}(x_j,t,\xi^{(i)})$ are respectively evaluated from the solution of the corresponding deterministic problem at the cell j in physical space computed with the deterministic solver and from the exact solution of the corresponding deterministic problem at the center of the cell j in physical space. Again, a sample set of size $M = 100\,000$ is used. In the right panel of Fig. 7, we compare the quantities $\epsilon^2_{ex,\mathrm{MC}}$ and ϵ^2_{ex} as a function of the spatial step. The observed order of convergence is 1, as expected for the present Roe-type finite volume scheme used for space discretization. All in all, the MC error is slightly smaller than the Galerkin error. Lastly, we have noticed that taking a constant Δt for the MC method corresponding to the time step of the Galerkin method produces the same results as the Galerkin method.

4.2. Test case 2: Euler equations

In this section, the method is tested on the stochastic Euler equations with one random parameter. The goal of this test case is to assess the method on a nonlinear hyperbolic system of conservation laws, so that the set of approximate eigenvectors of the Galerkin system is more complex than in the scalar case. Moreover, we propose a test case where sonic points appear just in a portion of the stochastic space. We consider the one-dimensional Sod shock tube problem, where the flow of an ideal gas is governed by the Euler equations. Conventional thermodynamic notation is used instead of the lower/upper case convention adopted previously. The conserved quantities are the fluid density ρ, the impulse $q = \rho v$ (with v the velocity), and the total energy $E = 1/2\rho v^2 + \rho e$, where the first term is the kinetic energy and the second one the internal energy (per unit volume). The tube extends over one unit of length and is opened at $x = 0$ and $x = 1$. The boundary conditions are $\frac{\partial \rho}{\partial x} = \frac{\partial q}{\partial x} = \frac{\partial E}{\partial x} = 0$ at both extremities of the tube. The discretization uses $\mathrm{Nc} = 250$ cells in physical space.

4.2.1. Problem definition

We consider an uncertainty on the initial Mach number parametrized by a unique random variable ξ having a uniform distribution in $[0, 1]$:

$$Ma^0(\xi) = \begin{cases} 0.7 + 0.5\xi & x \in [0, 1/4], \\ 2.46 \times (0.7 + 0.5\xi) & x \in (1/4, 1]. \end{cases} \tag{24}$$

We set

$$U(x,t,\xi) = (\rho(x,t,\xi), q(x,t,\xi), E(x,t,\xi)) \in \mathcal{A}_U \otimes L^2(\Xi, p_\xi), \tag{25}$$

where $\mathcal{A}_U \subset \mathbb{R}^3$ is the set of admissible states such that the density and the pressure are positive and

$$F(U;\xi) = (F_\rho(U;\xi), F_q(U;\xi), F_E(U;\xi)) = (q(\xi), (q^2/\rho + p)(\xi), (v(E+p))(\xi)) \in \mathbb{R}^3 \otimes L^2(\Xi, p_\xi), \tag{26}$$

with the pressure p given by the ideal gas law

$$p(\rho, q, E) = (\gamma - 1)\left(E - \frac{1}{2}\rho v^2\right), \tag{27}$$

and $\gamma = 1.4$ is the adiabatic coefficient. The other initial conditions are

$$p^0(x) = \begin{cases} 0.05 & x \in [0, 1/4], \\ 0.008 \times 0.05 & x \in (1/4, 1], \end{cases} \qquad \rho^0(x) = \begin{cases} 1.4 & x \in [0, 1/4], \\ 1.4 \times 0.03 & x \in (1/4, 1]. \end{cases} \tag{28}$$

Consequently, there is one stochastic dimension ($\mathrm{N} = 1$) and $\mathrm{P}_\pi = \mathrm{No} + 1$.

4.2.2. The numerical solver

At each physical interface, the numerical flux $\varphi^{\mathrm{DM}}(u_L, u_R)$ defined by (16) has to be evaluated. We approximate the stochastic quantities present in the numerical flux by their projection on $\mathcal{S}^{\mathrm{P}}$ that we compute in a pseudo-spectral way. To this end, we rely on [12], which describes tools for accurate evaluations of polynomial and non-polynomial functions of variables represented by stochastic expansions. For the Euler equations, the nonlinearities can be handled by the use of three pseudo-spectral stochastic operations, namely the pseudo-spectral product $*$, the pseudo-spectral inverse $^{-*}$ obtained from the resolution of a linear system, and the pseudo-spectral square root $^{*/2}$ obtained from the resolution of a nonlinear system (see [12,8]). The first component of $\varphi^{\mathrm{DM}}(u_L, u_R)$ is the Roe-type numerical flux $\varphi^{\mathrm{Roe}}(u_L, u_R)$ whose construction is detailed in [8]. We describe here the evaluation of the correction part of $\varphi^{\mathrm{DM}}(u_L, u_R)$ for the case of the Euler equations. To this end,

we need the approximate eigenvalues and right eigenvectors of a_{LR}^{Roe}. The Galerkin Jacobian matrix $\nabla_u f(u) \in \mathbb{R}^{3(\mathrm{P}+1),3(\mathrm{P}+1)}$ is approximated as

$$\nabla_u f(u) = \left\langle \nabla_U F(U^{\mathrm{P}};\cdot)\Psi_\alpha\Psi_\beta \right\rangle_{\alpha\beta} \approx \left(\sum_{\delta=1}^{\mathrm{P}} (\nabla_U F^*(U^{\mathrm{P}};\cdot))_\delta \mathcal{M}_{\alpha\beta\delta} \right)_{\alpha\beta}, \tag{29}$$

where $\nabla_U F^*(U^{\mathrm{P}};\xi)$ is the pseudo-spectral approximation of the projection of $\nabla_U F(\cdot;\xi)$ on $\mathcal{S}^{\mathrm{P}}$. Specifically, defining $H^* := (E^{\mathrm{P}} + p^*) * \rho^{-*}$, the pseudo-spectral approximation of the enthalpy on $\mathcal{S}^{\mathrm{P}}$, $\nabla_U F^*(U^{\mathrm{P}};\cdot)$ is defined as

$$\nabla_U F^*(U^{\mathrm{P}};\cdot) = \begin{pmatrix} 0 & 1 & 0 \\ 1/2(\gamma-3)(v^**v^*) & -(\gamma-3)v^* & \gamma-1 \\ 1/2(\gamma-1)(v^**(v^**v^*)) - v^**H^* & H^* - (\gamma-1)(v^**v^*) & \gamma v^* \end{pmatrix}. \tag{30}$$

Consequently, the eigenvalues of a_{LR}^{Roe} can be approximated by the approximation in $\mathcal{S}^{\mathrm{P}}$ of the stochastic eigenvalues of $\nabla_U F^*(U_{LR}^{\mathrm{Roe,P}}(\xi);\xi)$ at Gauss points in each stochastic element, that is,

$$(v_{LR}^{\mathrm{Roe},*} \pm c_{LR}^{\mathrm{Roe},*})(\xi_\eta)_{\eta=1,\dots,\mathrm{P}_\pi}, \quad \text{and} \quad v_{LR}^{\mathrm{Roe},*}(\xi_\eta)_{\eta=1,\dots,\mathrm{P}_\pi}, \tag{31}$$

where $v^{\mathrm{Roe}}(\xi)$ and $c^{\mathrm{Roe}}(\xi)$ are respectively the stochastic Roe velocity and corresponding sound velocity. Moreover, the eigenvectors of a_{LR}^{Roe} can be approximated by $(\omega_\eta R^{k,*}(\xi_\eta)\Psi_\beta)_{\beta,\eta=1,\dots,\mathrm{P}_\pi,k=1,2,3}$, where $(R^{k,*}(\xi))_{k=1,2,3}$ are the approximations in $\mathcal{S}^{\mathrm{P}}$ of the stochastic eigenvectors of $\nabla_U F^*(U_{LR}^{\mathrm{Roe,P}}(\xi);\xi)$, that is,

$$\begin{aligned} R^{1,*} &= (1,\, v^{\mathrm{Roe},*} + c^{\mathrm{Roe},*},\, H^{\mathrm{Roe},*} + v^{\mathrm{Roe},*} * c^{\mathrm{Roe},*})^T, \\ R^{2,*} &= (1,\, v^{\mathrm{Roe},*} - c^{\mathrm{Roe},*},\, H^{\mathrm{Roe},*} + v^{\mathrm{Roe},*} * c^{\mathrm{Roe},*})^T, \\ R^{3,*} &= (1,\, v^{\mathrm{Roe},*},\, H^{\mathrm{Roe},*} - (c^{\mathrm{Roe},*} * c^{\mathrm{Roe},*})/(\gamma-1))^T, \end{aligned} \tag{32}$$

where $H^{\mathrm{Roe},*}(\xi)$ is the pseudo-spectral approximation in $\mathcal{S}^{\mathrm{P}}$ of the stochastic Roe enthalpy. Thus, we have all the tools necessary for computing the intermediate states for all the left and right states (u_L, u_R). To determine the set of the sonic indices S', we use the approximate left and right eigenvalues $(v_L^* \pm c_L^*)(\xi_\eta)_{\eta=1,\dots,\mathrm{P}_\pi}$ and $v_L^*(\xi_\eta)_{\eta=1,\dots,\mathrm{P}_\pi}$, that we compare with $(v_R^* \pm c_R^*)(\xi_\eta)_{\eta=1,\dots,\mathrm{P}_\pi}$ and $v_R^*(\xi_\eta)_{\eta=1,\dots,\mathrm{P}_\pi}$.

4.2.3. Results

In this section we present and analyze the results for the shock tube problem with uncertainty in the initial Mach number. We begin with a general analysis of the results, taking $\mathrm{No} = 2$ and $\mathrm{Nr} = 3$ as stochastic discretization parameters, so that the dimension of the stochastic space is 24.

In the deterministic case and for the initial condition (28) for a certain realization of $Ma^0(\xi)$, a shock wave generated at the discontinuity travels to the right with velocity $v + c$, while a rarefaction fan travels to the left with velocity $v - c$, and a contact discontinuity wave travels to the right with velocity v. Here, the uncertain initial Mach number will affect the propagation velocity of the shock, contact discontinuity, and rarefaction fan. Solutions for different realizations of $Ma^0(\xi)$ exhibit patterns similar to those in the deterministic case, but with different slopes for the shock, contact discontinuity, and rarefaction fan. Moreover, the uncertainty in the initial Mach number is such that sonic points are generated only for $\xi \in [0, 0.6]$. To assess the validity of the stochastic expansion and the effectiveness of the DM-type entropy corrector, we show in Fig. 8 a reconstruction of the stochastic density $\rho(x,t,\xi)$ at $t = 1$ obtained without (left) and with (right) the entropy corrector. In the left panel, we observe that an entropy-violating shock is generated in the vicinity of $x = 0.2$ for $\xi \in [0, 0.6]$, while for $\xi \in [0.6, 1]$ the expansion wave is well-captured. When using the DM-type entropy corrector in the right panel of Fig. 8, the sonic expansion wave is also well-captured, even if a small jump remains due to the first-order nature of the numerical scheme. As for the Burgers equation (see the left panel of Fig. 6), this jump converges to zero at first order with the spatial step Δx. We also observe that the solver captures well the discontinuity in physical as well as in stochastic space in the vicinity of the shock wave; this point has already been investigated in [8].

We compare in Fig. 9, at $t = 1$, the mean and standard deviation of the density computed with the Galerkin method with that computed with a MC method where deterministic (discrete) Euler problems corresponding to a sample set of size 10 000 are solved. Following the remarks in Section 4.1.3, we compute the solution for the two methods with a fixed time step Δt; this time step is for simplicity the minimum of the time steps obtained in the Galerkin solver. We notice that the means and standard deviations are in excellent agreement.

We will not study the stochastic convergence with respect to the stochastic parameters No, Nr, since a study has already been provided in [8]. Nevertheless, we can mention that for this test case, a low resolution level is sufficient to capture the sonic expansion wave, while a higher resolution level is needed in the vicinity of the shock wave to capture the discontinuity in the stochastic space. This fact corroborates the need for stochastic adaptivity, which is the focus of ongoing efforts.

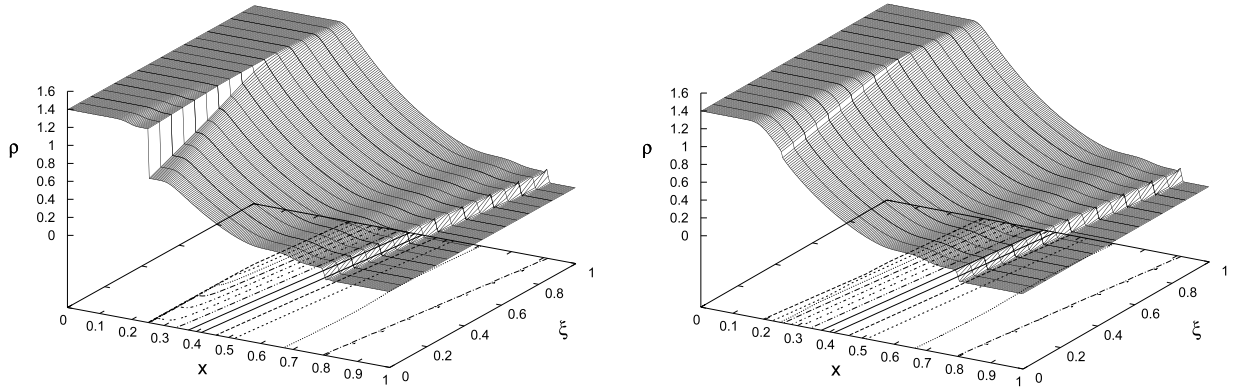

Fig. 8. Reconstruction of the stochastic density $\rho(x, t, \xi)$ at $t = 1$ obtained without (left) and with (right) the entropy corrector. The computations were with Nr = 3 and No = 2.

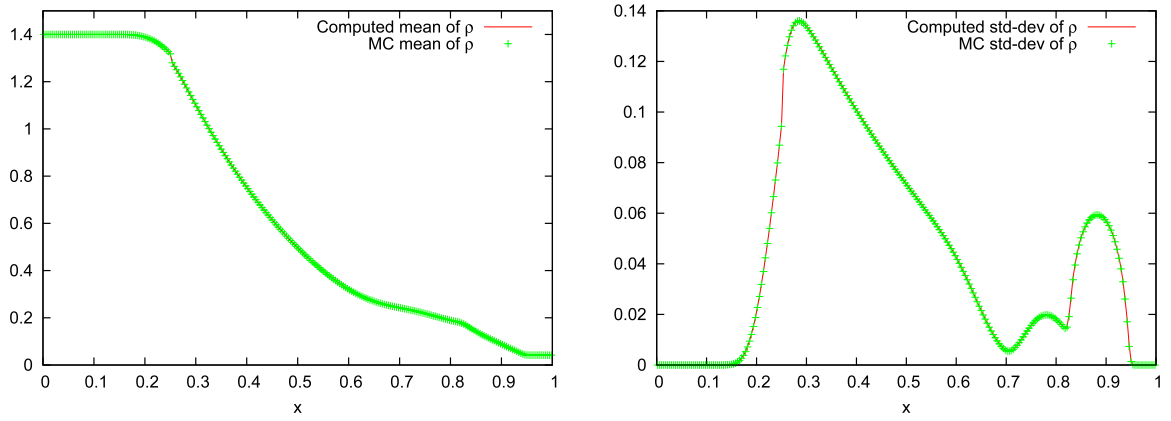

Fig. 9. Comparison of the means and standard deviations of the numerical density, at $t = 1$, computed with a Galerkin method (using Nr = 3 and No = 2) and a MC method (using a sample set of size 10 000).

4.2.4. CPU improvements

We describe in this section a way to improve cost-effectiveness in the detection of sonic points. To illustrate our idea, we show in Fig. 10, at $t = 1$ and for selected interfaces at various positions in physical space, the approximate eigenvalues $(v_{LR}^{\mathrm{Roe},*} \pm c_{LR}^{\mathrm{Roe},*})(\xi_\eta)_{\eta=1,\ldots,\mathrm{P}_\pi}$ and $v_{LR}^{\mathrm{Roe},*}(\xi_\eta)_{\eta=1,\ldots,\mathrm{P}_\pi}$ corresponding to each stochastic element and the associated density functions. This figure deserves several comments. First, we notice that the density functions have completely different patterns for the different interfaces considered. For $x = 0.15$, $x = 0.2$, and $x = 0.25$, the sets of eigenvalues corresponding to $v - c$, v, and $v + c$ have distinct supports, while these sets have overlapping supports for $x = 0.9$ (and are therefore represented in three different panels in the bottom row of Fig. 10). For the interface $x = 0.9$, which is affected by the shock wave, it is interesting to notice that each set of eigenvalues can be split into two different subsets, except for a few eigenvalues which actually correspond to the discontinuity in the stochastic space. In contrast, for the three panels in the upper row, the eigenvalues of each stochastic element are very close and the density functions hit their maximum values where the eigenvalues are practically equal, that is, for the stochastic elements supporting a low variability. This phenomenon is particularly visible at $x = 0.2$ and $x = 0.25$. Moreover, the plateaus in the density function correspond to stochastic elements where the eigenvalues have locally uniform distributions. A further important remark is that the first three panels correspond to positions located in the vicinity of the sonic points, and only the eigenvalues $(v_{LR}^{\mathrm{Roe},*} - c_{LR}^{\mathrm{Roe},*})(\xi_\eta)_{\eta=1,\ldots,\mathrm{P}_\pi}$ can take negative values. Therefore, the key point for reducing the computational time is to test the detection of sonic points only using the eigenvalues $(v_{LR}^{\mathrm{Roe},*} - c_{LR}^{\mathrm{Roe},*})(\xi_\eta)_{\eta=1,\ldots,\mathrm{P}_\pi}$. To further reduce the CPU time, we only test for each stochastic element α_σ, $1 \le \alpha_\sigma \le \mathrm{P}_\sigma$, whether the mean $E^{\alpha_\sigma}[v_{LR}^{\mathrm{Roe},*} - c_{LR}^{\mathrm{Roe},*}]$ changes its sign at the interface, in other words, whether

$$E^{\alpha_\sigma}[(v_L^* - c_L^*)] - \mathrm{ctol} * v_{\mathrm{ref}} < 0 < E^{\alpha_\sigma}[(v_R^* - c_R^*)] + \mathrm{ctol} * v_{\mathrm{ref}}, \quad 1 \le \alpha_\sigma \le \mathrm{P}_\sigma, \tag{33}$$

where ctol is a fixed parameter and v_{ref} is a reference velocity here taken equal to 1 as reflected in the size of eigenvalues reported in Fig. 11.

We show in Fig. 10 the portion of the domain (x, ξ) which is actually selected for the entropy correction and the number of sonic points detected (card S') for two different values of the parameter ctol. For ctol $= 10^{-2}$ (left), we observe a rectangular

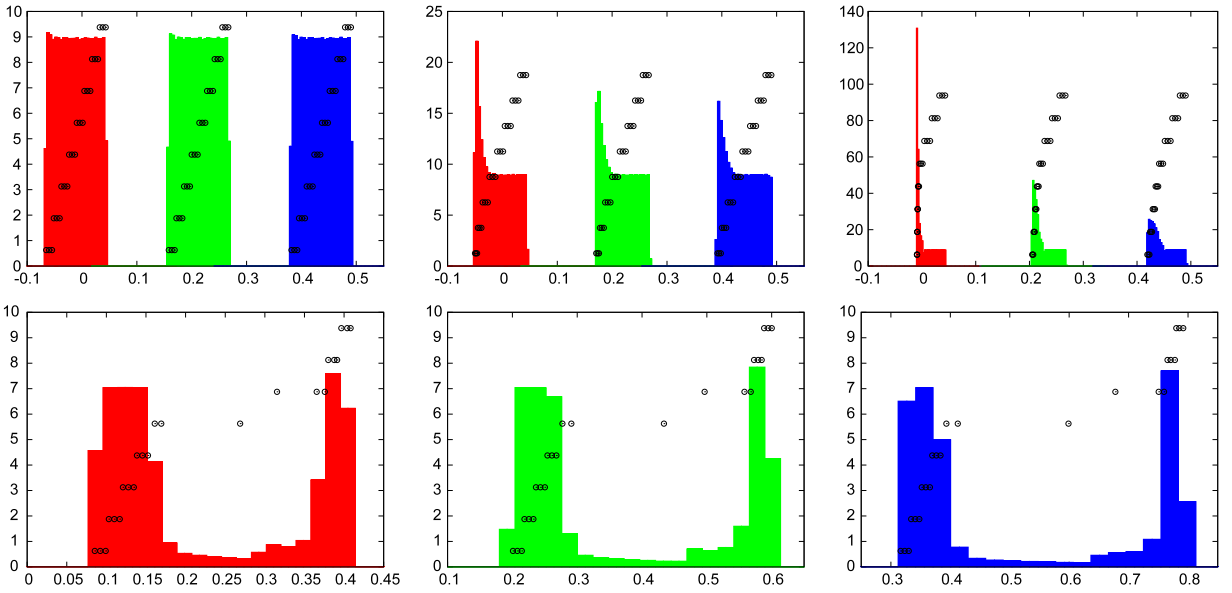

Fig. 10. Approximate eigenvalues $(v_{LR}^{\mathrm{Roe},*} - c_{LR}^{\mathrm{Roe},*})(\xi_\eta)_{\eta=1,\ldots,\mathrm{P}_\pi}$ (red/gray), $v_{LR}^{\mathrm{Roe},*}(\xi_\eta)_{\eta=1,\ldots,\mathrm{P}_\pi}$ (green/light gray), and $(v_{LR}^{\mathrm{Roe},*} + c_{LR}^{\mathrm{Roe},*})(\xi_\eta)_{\eta=1,\ldots,\mathrm{P}_\pi}$ (blue/dark gray) corresponding to each stochastic element together with their density functions for $x = 0.15$, $x = 0.2$, $x = 0.25$ (top), and $x = 0.9$ (bottom). The presented results correspond to $t = 1$ and the computations were with Nr $= 3$ and No $= 2$. (For interpretation of the references to colour in this figure legend, the reader is referred to the web version of this article.)

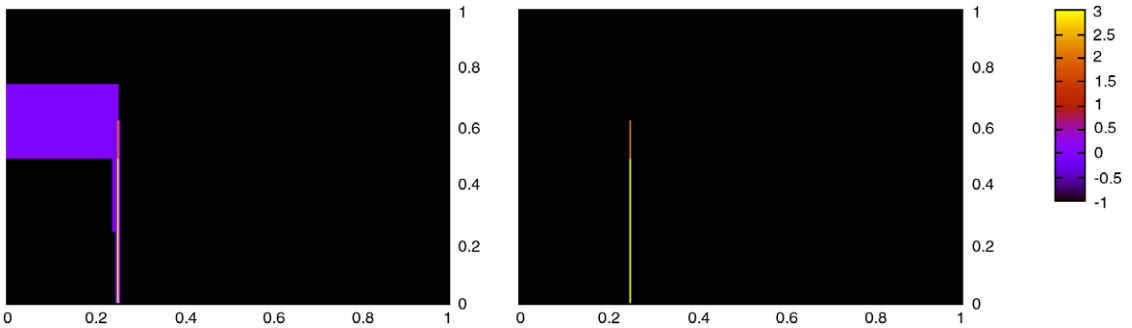

Fig. 11. Portion of the domain (x, ξ) where the entropy correction is applied. The color coding corresponds to a value equal to -1 for areas where no correction is tested and a value equal to card S' otherwise. Therefore, a value 0 implies that no correction was actually needed. The computations were with ctol $= 10^{-2}$ (left) and ctol $= 10^{-5}$ (right).

Table 1
Normalized computational times T_{CPU}, fraction *factor* of stochastic cells actually tested, and error measure ϵ_h for different stochastic discretization parameters Nr and No.

dim $\mathcal{S}^{\mathrm{No,Nr}}$	No $= 1$, Nr $= 3$		No $= 2$, Nr $= 3$		No $= 3$, Nr $= 3$	
	16		24		32	
	T_{CPU}	*factor*	T_{CPU}	*factor*	T_{CPU}	*factor*
ctol $= +\infty$	11.7	1.0e−0	16.1	1.0e−0	21.6	1.0e−0
ctol $= 10^{-1}$	8.2	3.7e−1	11.8	3.7e−1	16.4	3.7e−1
ctol $= 10^{-2}$	6.5	7.1e−2	9.8	7.1e−2	13.9	7.1e−2
ctol $= 10^{-3}$	6.1	2.8e−3	9.3	2.8e−3	13.5	2.8e−3
ctol $= 0$	6	2.5e−3	9.2	2.5e−3	13.4	2.5e−3
ϵ_h	1.32e−3		7.17e−4		2.88e−4	

portion of the domain on the left which is positive for the test (33) but does not actually correspond to sonic points. The flagged interfaces correspond in fact to the portion of the domain where the initial condition passes from the sonic case to the subsonic case. For both cases, three sonic points are detected in the four stochastic elements corresponding to $\xi \in [0, 0.5]$, and two sonic points are detected in the fifth stochastic element.

To complete the discussion, we provide an estimate of the CPU times in Table 1. CPU times (T_{CPU}) are reported for an integration of the Euler equations up to $t = 1$ on a fixed grid having Nc $= 250$ cells, and are normalized by the computational

Table 2
Fraction of computational time spent for the entropy correction, $R_{\text{cor}}(\text{ctol})$, for different values of the expansion order No and parameter ctol.

$\dim \mathcal{S}^{\text{No,Nr}}$	No = 1, Nr = 3 16	No = 2, Nr = 3 24	No = 3, Nr = 3 32
$\text{ctol} = +\infty$	0.49	0.42	0.38
$\text{ctol} = 10^{-1}$	0.19	0.16	0.14
$\text{ctol} = 10^{-2}$	0.04	0.03	0.02

time using No = Nr = 0 and ctol = $+\infty$, i.e. for the deterministic problem for which the entropy correction is tested everywhere. We observe that the above ideas enable us to save a considerable amount of CPU time since the CPU time can be divided by a factor of 2 for No and Nr fixed. Moreover, we indicate the fraction of stochastic cells which are actually tested for the correction. This quantity does not change significantly when decreasing ctol below 10^{-3}. We define the error measure on the density as

$$\epsilon_h^2(t) \equiv \frac{1}{M}\sum_{i=1}^{M}\sum_{j=1}^{\text{Nc}} \Delta x \left(\rho_j^{\text{No,Nr}}(t,\xi^{(i)}) - \rho_j^{\text{MC}}(t,\xi^{(i)})\right)^2, \tag{34}$$

where, for each element $\xi^{(i)}$ in a sample set, $\rho_j^{\text{No,Nr}}(t,\xi^{(i)})$ and $\rho_j^{\text{MC}}(t,\xi^{(i)})$ are respectively evaluated from the computed solution at the cell j in physical space and from the solution of the corresponding deterministic problem at the cell j in physical space computed with the deterministic solver. We use a sample set of size $M = 100\,000$ uniformly drawn from Ξ. In this specific case, we observe that the value of ctol does not affect the error. This confirms that a criterion based on the averaged velocity over the stochastic element considered is sufficient.

We close the discussion on CPU times with a brief estimate of the computational overhead resulting from the entropy correction. To this end, we evaluate the CPU time dedicated to entropy correction by computing the ratio

$$R_{\text{cor}}(\text{ctol}) = \frac{T_{\text{CPU}}(\text{ctol}) - T_{\text{CPU}}(\text{ctol}=0)}{T_{\text{CPU}}(\text{ctol}=+\infty)}. \tag{35}$$

Since for ctol = 0, the set of interfaces where the correction is tested is a negligible fraction of the full set of interfaces, $T_{\text{CPU}}(\text{ctol}=0)$ is essentially equal to the CPU time for the Roe solver without entropy correction. In contrast, $T_{\text{CPU}}(\text{ctol} = +\infty)$ is the computational time when the set of sonic points is determined for all interfaces. Therefore $R_{\text{cor}}(\text{ctol})$ is the fraction of CPU time spent on entropy correction in the flux computation. Values for $R_{\text{cor}}(\text{ctol})$ are reported in Table 2 for different values of ctol, expansion orders No, and a fixed resolution level Nr = 3. The first line, corresponding to ctol = $+\infty$, shows that the entropy correction yields a significant computational overhead when tested everywhere. Interestingly, when the expansion order No increases, $R_{\text{cor}}(\text{ctol} = +\infty)$ decreases, indicating that for a given interface, the computation of the Roe part of the flux becomes relatively more demanding than its corrective part. This trend can be attributed to the pseudo-spectral computations, and, therefore, depends on the conservative system under scrutiny, and more specifically on the nonlinearities involved in the flux functions. In addition, Table 2 indicates that lowering ctol allows us to drastically reduce the entropy correction overhead: for ctol = 10^{-2}, only a marginal amount of the total CPU time is spent on the entropy correction.

5. Conclusion and discussion

We have proposed an extension of the entropy corrector of Dubois and Mehlman [15] to the computation of the numerical Roe flux for the Galerkin system arising from the projection of stochastic hyperbolic equations. The proposed method relies on approximate eigenvalues and eigenvectors of the Roe Galerkin Jacobian matrix using the underlying Gauss quadrature points and weights, thereby avoiding the need for the costly decomposition of the Roe Galerkin Jacobian matrix. In addition, such a procedure can be applied to the case of non-strictly hyperbolic systems since it provides an unambiguous relation between the eigenvalues, eigenvectors and reconstructed intermediate states. Numerical tests for the Burgers and Euler equations have demonstrated the effectiveness of the proposed corrector in providing entropy solutions. A robust criterion has also been presented for the *a priori* localization of the physical cell interfaces requiring a correction, yielding a significant reduction of the corrector computational overhead.

The present corrector still involves some limitations that will have to be overcome for handling general situations. Firstly, the corrector, as well as the Roe Galerkin solver, assumes the availability of the explicit expressions for the stochastic eigenvalues and eigenvectors of the stochastic hyperbolic system. This is not a limitation for the Burgers and Euler equations. However, for general systems of conservation laws, *a priori* knowledge of the solution characteristics may not be available. Alternative strategies for dealing with such general problems are still an open question. Secondly, the approximate eigenvalues and eigenvectors of the Roe Galerkin Jacobian matrix assume a fully tensorized polynomial basis associated with each stochastic element for constructing the corresponding set of Gauss points and weights. For problems involving a large number of random variables, sparse polynomial bases are mandatory for tempering the curse of dimensionality. Such bases prevent the immediate construction of approximate eigenvalues and eigenvectors as above. In [8], we have shown that for

partially tensorized stochastic bases, the computation of the upwind matrix can still be performed using the set of fully tensorized Gauss points. A similar approach could be followed for the correction: whenever a sonic point is detected on a physical interface, the left and right Galerkin states could be locally lifted to the (higher dimensional) fully tensorized stochastic approximation space in which the flux correction can be determined by means of the present method, before being projected back to the original sparse stochastic space. Owing to the pertinent criteria proposed for the detection of sonic points, these lifting/projection procedures would not be used frequently, so this approach would not incur significant computational overheads. Such a procedure however remains to be implemented and tested.

Finally, we observe that the proposed Roe solver and entropy corrector require sufficient stochastic resolution to properly capture solution discontinuities in the stochastic space. Results presented here and in [8] use a uniform stochastic refinement, while in fact the solutions are essentially smooth everywhere except in the vicinity of localized shocks and discontinuities. This observation calls for the use of adaptive methods where the stochastic resolution (and possibly also the spatial one) is selected with regard to the local smoothness of the solution in order to optimize the computational effort. In doing this, the tensorized structure of the deterministic (spatial) and stochastic approximation spaces will be lost. Current research focuses on the implementation of such adaptive strategies, with particular emphasis on the derivation of robust error estimators in order to drive the refinement (and coarsening) of the discretization spaces.

Appendix. $\mathbb{R}$-diagonalization of the approximate Galerkin Jacobian matrix

Since the matrix $\overline{\nabla_u f}$ is block-diagonal, we focus on a single stochastic element and drop the index α_σ. Moreover, we only consider right eigenvectors; the proof for left eigenvectors is similar. Let $k = 1, \dots, m$ and let $\eta = 1, \dots, \mathrm{P}_\pi$. Let $V_{k\eta}(\xi)$ be the $\mathbb{R}^m$-valued interpolation polynomial of degree less than or equal to No such that for all $\gamma = 1, \dots, \mathrm{P}_\pi$,

$$V_{k\eta}(\xi_\gamma) = \delta_{\eta\gamma} R^k(\xi_\gamma),$$

where $\delta_{\eta\gamma}$ denotes the Kronecker symbol. Then, denoting by $\langle \cdot, \cdot \rangle$ the $L^2(\Xi, p_\xi)$-scalar product and observing that the quadrature is exact for polynomials up to degree $2\mathrm{No} + 1$, we obtain for all $\beta = 1, \dots, \mathrm{P}_\pi$,

$$\langle \Psi_\beta, V_{k\eta} \rangle = \sum_{\gamma=1}^{\mathrm{P}_\pi} \varpi_\gamma \Psi_\beta(\xi_\gamma) V_{k\eta}(\xi_\gamma) = \varpi_\eta \Psi_\beta(\xi_\eta) R^k(\xi_\eta) = (r'_{k\eta})_\beta.$$

Since the basis $(\Psi_\beta)_{\beta=1,\dots,\mathrm{P}_\pi}$ is $L^2(\Xi, p_\xi)$-orthogonal, this yields for all $\xi \in \Xi$,

$$V_{k\eta}(\xi) = \sum_{\beta=1}^{\mathrm{P}_\pi} (r'_{k\eta})_\beta \Psi_\beta(\xi). \tag{36}$$

Let now $\alpha = 1, \dots, \mathrm{P}_\pi$. We observe that

$$\begin{aligned}
(\overline{\nabla_u f} r'_{k\eta})_\alpha &= \sum_{\beta=1}^{\mathrm{P}_\pi} \left(\sum_{\gamma=1}^{\mathrm{P}_\pi} \varpi_\gamma \nabla_U F(U^{\mathrm{P}}(\xi_\gamma); \xi_\gamma) \Psi_\alpha(\xi_\gamma) \Psi_\beta(\xi_\gamma) \right) (r'_{k\eta})_\beta \\
&= \sum_{\gamma=1}^{\mathrm{P}_\pi} \varpi_\gamma \nabla_U F(U^{\mathrm{P}}(\xi_\gamma); \xi_\gamma) \Psi_\alpha(\xi_\gamma) \left(\sum_{\beta=1}^{\mathrm{P}_\pi} (r'_{k\eta})_\beta \Psi_\beta(\xi_\gamma) \right) \\
&= \sum_{\gamma=1}^{\mathrm{P}_\pi} \varpi_\gamma \nabla_U F(U^{\mathrm{P}}(\xi_\gamma); \xi_\gamma) \Psi_\alpha(\xi_\gamma) V_{k\eta}(\xi_\gamma),
\end{aligned}$$

where we have used (36) at ξ_γ. Hence, since $V_{k\eta}(\xi_\gamma) = \delta_{\gamma\eta} R^k(\xi_\eta)$ and $R^k(\xi_\eta)$ is a right eigenvector of $\nabla_U F(U^{\mathrm{P}}(\xi_\eta); \xi_\eta)$, we infer

$$(\overline{\nabla_u f} r'_{k\eta})_\alpha = \varpi_\eta \nabla_U F(U^{\mathrm{P}}(\xi_\eta); \xi_\eta) R^k(\xi_\eta) \Psi_\alpha(\xi_\eta) = \varpi_\eta \Lambda^k(\xi_\eta) R^k(\xi_\eta) \Psi_\alpha(\xi_\eta) = \lambda_{k\eta} (r'_{k\eta})_\alpha.$$

To close the proof, it remains to verify that the family $(r'_{k\eta})_{k=1,\dots,m,\eta=1,\dots,\mathrm{P}_\pi}$ forms a complete basis of $\mathbb{R}^{m\mathrm{P}_\pi}$. Indeed, let $m\mathrm{P}_\pi$ real numbers $(a_{k\eta})_{k=1,\dots,m,\eta=1,\dots,\mathrm{P}_\pi}$ be such that $\sum_{k=1}^m \sum_{\eta=1}^{\mathrm{P}_\pi} a_{k\eta} r'_{k\eta} = 0$. Consider the stochastic vector

$$A(\xi) = \sum_{k=1}^m \sum_{\eta=1}^{\mathrm{P}_\pi} \sum_{\beta=1}^{\mathrm{P}_\pi} a_{k\eta} (r'_{k\eta})_\beta \Psi_\beta(\xi).$$

Evaluating this vector at ξ_γ for any $\gamma = 1, \dots, \mathrm{P}_\pi$ yields

$$A(\xi_\gamma) = \sum_{k=1}^m \sum_{\eta=1}^{\mathrm{P}_\pi} a_{k\eta} \left(\sum_{\beta=1}^{\mathrm{P}_\pi} (r'_{k\eta})_\beta \Psi_\beta(\xi_\gamma) \right) = \sum_{k=1}^m \sum_{\eta=1}^{\mathrm{P}_\pi} a_{k\eta} V_{k\eta}(\xi_\gamma),$$

owing to (36) so, by definition of $V_{k\eta}$,

$$A(\xi_\gamma) = \sum_{k=1}^{m} a_{k\gamma} R^k(\xi_\gamma).$$

Since the vector $A(\xi_\gamma)$ is assumed to be zero and since $(R^k(\xi_\gamma))_{k=1,\dots,m}$ forms a complete basis of $\mathbb{R}^m$ by assumption, this yields $a_{k\gamma} = 0$ for all $k = 1, \dots, m$. Since γ is arbitrary, this completes the proof.

References

[1] R. Ghanem, P. Spanos, Stochastic Finite Elements: A Spectral Approach, Dover, 2003.
[2] G. Lin, C.-H. Su, G.E. Karniadakis, Stochastic modeling of random roughness in shock scattering problems: theory and simulations, Comput. Methods Appl. Mech. Engrg. 197 (43–44) (2008) 3420–3434.
[3] R. Abgrall, A simple, flexible and generic deterministic approach to uncertainty quantifications in non linear problems: application to fluid flow problems, Rapport de recherche INRIA, 00325315, 2008.
[4] L. Ge, K.F. Cheung, M.H. Kobayashi, Stochastic solution for uncertainty propagation in nonlinear shallow-water equations, J. Hydraul. Eng. (2008) 1732–1743.
[5] G. Poette, B. Després, D. Lucor, Uncertainty quantification for systems of conservation laws, J. Comput. Phys. 228 (7) (2009) 2443–2467.
[6] D. Gottlieb, D. Xiu, Galerkin method for wave equations with uncertain coefficients, Commun. Comput. Phys. 3 (2) (2008) 505–518.
[7] G. Lin, C.-H. Su, G.E. Karniadakis, Predicting shock dynamics in the presence of uncertainties, J. Comput. Phys. 217 (1) (2006) 260–276.
[8] J. Tryoen, O. Le Maître, M. Ndjinga, A. Ern, Intrusive Galerkin methods with upwinding for uncertain nonlinear hyperbolic systems, J. Comput. Phys. 229 (2010) 6485–6511.
[9] M. Deb, I. Babuška, J. Oden, Solution of stochastic partial differential equations using Galerkin finite element techniques, Comput. Methods Appl. Mech. Engrg. 190 (48) (2001) 6359–6372.
[10] O. Le Maître, H. Najm, R. Ghanem, O. Knio, Multi-resolution analysis of Wiener-type uncertainty propagation schemes, J. Comput. Phys. 197 (2) (2004) 502–531.
[11] X. Wan, G.E. Karniadakis, Multi-element generalized polynomial chaos for arbitrary probability measures, SIAM J. Sci. Comput. 28 (3) (2006) 901–928 (electronic).
[12] B. Debusschere, H. Najm, P. Pébay, O. Knio, R. Ghanem, O. Le Maître, Numerical challenges in the use of polynomial chaos representations for stochastic processes, SIAM J. Sci. Comput. 26 (2) (2004) 698–719.
[13] A. Harten, High resolution schemes for hyperbolic conservation laws, J. Comput. Phys. 49 (3) (1983) 357–393.
[14] P. Roe, Some contributions to the modelling of discontinuous flows, in: Large-scale Computations in Fluid Mechanics, Part 2, La Jolla, Calif., 1983, in: Lectures in Appl. Math., vol. 22, Amer. Math. Soc., Providence, RI, 1985, pp. 163–193.
[15] F. Dubois, G. Mehlman, A non-parameterized entropy correction for Roe's approximate Riemann solver, Numer. Math. 73 (2) (1996) 169–208.